In Vivo Characterization of a Series of ^{18}F-Diaryl Sulfides (^{18}F-2-(2′-((Dimethylamino)Methyl)-4′-(Fluoroalkoxy)Phenylthio)Benzenamine) for PET Imaging of the Serotonin Transporter

Julie L. Wang[1], Ajit K. Parhi[2], Shunichi Oya[2], Brian Lieberman[2], and Hank F. Kung[1,2]

[1]Department of Pharmacology, School of Medicine, University of Pennsylvania, Philadelphia, Pennsylvania; and [2]Department of Radiology, School of Medicine, University of Pennsylvania, Philadelphia, Pennsylvania

PET of the serotonin transporter (SERT) in the brain is a useful tool for examining normal physiologic functions as well as disease states involving the serotonergic system. The goal of this study was to further develop and refine a series of 4′-fluoroalkoxy–substituted, ^{18}F-radiolabeled SERT imaging agents. 2-(2′-((Dimethylamino)methyl)-4′-(4-^{18}F-fluorobutoxy)phenylthiol)-benzenamine (**3**) and 2-(2′-((dimethylamino)methyl)-4′-(5-^{18}F-fluoropentoxy)phenylthiol)benzenamine (**4**) were synthesized and evaluated along with 2 previously reported compounds of this series, 2-(2′-((dimethylamino)methyl)-4′-(2-^{18}F-fluoroethoxy)-phenylthiol)benzenamine (**1**) and 2-(2′-((dimethylamino)methyl)-4′-(3-^{18}F-fluoropropoxy)phenylthiol)benzenamine (**2**). **Methods:** The in vitro binding affinities of compounds **3** and **4** were determined in monoamine transporter–transfected LLC-PK$_1$ cell homogenates. In vivo localization of the respective ^{18}F-labeled compounds was evaluated by biodistribution studies in male Sprague–Dawley rats. Compound **3** was selected for further examination by autoradiographic and PET studies in rats. **Results:** The corresponding mesylate precursors of **3** and **4** were radiolabeled with ^{18}F within 75–90 min. Radiochemical yield was 6%−35%, specific activity was 15–170 GBq/μmol, and radiochemical purity was greater than 97% (end of synthesis). The compounds showed subnanomolar binding affinities for SERT (inhibition constants, 0.51 and 0.76 nM, respectively), had brain uptake at 2 min of 1.25 and 0.68 percentage injected dose per gram, respectively, and possessed high target-to-nontarget (hypothalamus-to-cerebellum) ratios at 120 min after injection (6.51 and 5.70, respectively). Autoradiographic studies of ^{18}F-**3** showed selective localization in SERT-rich brain regions. PET studies of ^{18}F-3 showed clear localization in the midbrain, thalamus, and striatum. **Conclusion:** This compound series was found to have potential for producing a suitable ^{18}F-radiolabeled PET radiotracer for SERT. Compound **4**, the pentoxy derivative, had the lowest brain uptake and target-to-nontarget ratio. Compound **3**, the butoxy derivative, had a lower target-to-nontarget ratio than compounds **1** (ethoxy derivative) and 2 (propoxy derivative). Compounds **1** and **2** both hold promise as SERT radioimaging agents, but because of cost limitations, only compound **2** will be evaluated in further studies.

Key Words: brain imaging; radioligand; SERT; 5-HTT; ^{18}F

J Nucl Med 2009; 50:1509–1517
DOI: 10.2967/jnumed.108.060723

Received Nov. 30, 2008; revision accepted May 22, 2009.
For correspondence or reprints contact: Hank F. Kung, Department of Radiology, School of Medicine, University of Pennsylvania, 3700 Market St., Suite 305, Philadelphia, PA 19104.
E-mail: kunghf@gmail.com

The serotonin transporter (SERT) is located on the presynaptic terminals and cell bodies of serotonergic neurons in the brain. SERT functions as the main mechanism for terminating the action of serotonin. It transports the neurotransmitter serotonin in the synaptic cleft back into the neuron terminal and, consequently, prevents the action of serotonin at its postsynaptic receptors. Because it is believed that lower serotonin levels are a cause of or are associated with depression, blocking serotonin reuptake by use of SERT to increase synaptic serotonin levels has been applied in the treatment of depression. SERT is currently the site of drug action for the most commonly prescribed antidepressants, the selective serotonin reuptake inhibitors (*1,2*).

SERT imaging may then be useful in measuring drug occupancy by the selective serotonin reuptake inhibitors and may help in optimizing antidepressant drug therapy (*3–5*). In a broader scope, because of the location of SERT on the neuron, SERT can be used as a marker for the in vivo examination of serotonergic neuron integrity. The ability to image SERT in the brain is then a useful means for studying the many normal functions as well as disease states involving the serotonergic system in vivo (*6–9*). Thus, there is considerable interest in developing SERT radioligands for this purpose. *N,N*-^{11}C-dimethyl-2-(2-amino-4-cyanophenylthio)benzylamine (^{11}C-DASB) (Fig. 1), a diaryl sulfide derivative, is

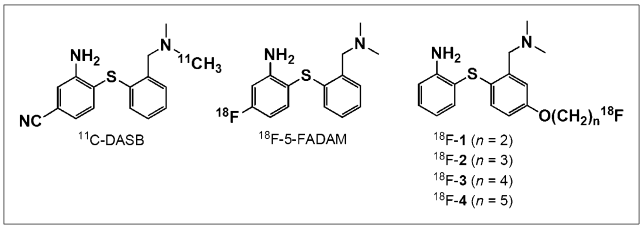

FIGURE 1. Molecular structures of selected SERT radioligands for PET.

currently the ligand of choice (*10,11*), but the major drawback of ^{11}C-DASB is the 20-min half-life ($t_{1/2}$) of ^{11}C, which limits its use to facilities possessing an on-site cyclotron and radiochemistry team.

Significant efforts in the development of ^{18}F ($t_{1/2}$, 109 min)-labeled SERT tracers based on various core structures have been made (*12–17*). However, there has been limited success because of suboptimal ligand properties or poor radiochemical yields. *N,N*-Dimethyl-2-(2-amino-4-^{18}F-fluorophenylthio)-benzylamine (^{18}F-5-FADAM) (Fig. 1), also a diaryl sulfide derivative, is a promising candidate, but the preparation of this agent requires a nucleophilic substitution of ^{18}F at a less activated 5-position on the aromatic ring. This problem contributes to a low radiochemical yield (<5%) (*17*), making this radiotracer less practical for routine clinical use. To overcome this problem, a novel series of SERT ligands with alkoxy substituents at the 4′-position on the other phenyl ring of the diaryl sulfide core (Fig. 1) were synthesized. This substitution at the 4′-position allows for a simple nucleophilic ^{18}F fluorination reaction. Other core structures used for alkoxy substitution in the past included nitroquipazines (*18*) and tropanes (*19*). However, there are several important benefits of the diaryl sulfide core structure: compounds of this class have demonstrated high affinity and selectivity for SERT; they are comparatively easy to synthesize; they have no optical center; and their small size (molecular mass of <650 g/mol) facilitates passage through the blood–brain barrier. Thus, many diaryl sulfide derivatives have been prepared and tested, but so far there has been a lack of progress in finding a suitable ^{18}F-labeled SERT imaging agent that can be prepared in high radiochemical yields.

Two promising candidates, 2-(2′-((dimethylamino)methyl)-4′-(2-^{18}F-fluoroethoxy)phenylthiol)benzenamine (**1**) and 2-(2′-((dimethylamino)methyl)-4′-(3-^{18}F-fluoropropoxy)-phenylthio)benzenamine (**2**) (Fig. 1), were recently reported (*20,21*). Previous attempts had focused on ring A substitutions. With compounds **1** and **2** it was found that ring B substitutions at the 4′-position could potentially yield an improved PET radiotracer for SERT. They were observed to have high SERT-binding affinity, good brain uptake, selective regional brain localization, and a high target-to-nontarget ratio. Importantly, because the fluoroalkoxy substituent was located at the 4′-position, compounds **1** and **2** were also relatively easy to radiolabel with ^{18}F in comparison with 5-FADAM. These positive results prompted further evaluation of **1** and **2** as well as attempts to refine this series by the synthesis and examination of compounds **3** and **4**. It can be predicted that the simple modification of increasing the 4′-fluoroalkoxy chain will result in higher lipophilicity, but the effects of this change on other properties, such as brain uptake and target-to-nontarget ratios, are less clear. This report provides additional datasets to aid in the selection of the best candidate(s) of the fluoroalkoxy series for future development.

MATERIALS AND METHODS

General

All reagents used for chemical synthesis were commercial products and were used without further purification unless otherwise indicated. Flash chromatography was performed by use of silica gel (230–400 mesh; Sigma-Aldrich). ^{1}H nuclear magnetic resonance (NMR) spectra were obtained at 200 MHz (Bruker DPX spectrometer). Chemical shifts were reported as δ values (ppm) relative to internal tetramethylsilane. Coupling constants were reported in hertz. The multiplicity was defined by s (singlet), d (doublet), t (triplet), br (broad), or m (multiplet). High-resolution mass spectroscopy (HRMS) were determined in experiments performed at the University of Pennsylvania.

Male Sprague–Dawley rats (180–390 g) were used in the relevant studies. All protocols requiring the use of rats were reviewed and approved by the Animal Care and Use Committee at the University of Pennsylvania. Rats were anesthetized by inhalation of 1.5%−2.5% isoflurane before any injections, before sacrifice, and during the length of PET. LLC-PK$_1$ cells expressing SERT, the norepinephrine transporter (NET), or the dopamine transporter (DAT) were kindly provided by Dr. Gary Rudnick (Yale University). (+)-McN5652 and nisoxetine were obtained from the National Institute of Mental Health chemical synthesis and drug supply program, and GBR12909 was obtained from Sigma-RBI. Escitalopram was considerately provided by Dr. Irwin Lucki (University of Pennsylvania). (5-iodo-2-[[2-2-[(dimethylamino)methyl]phenyl]thio]benzyl alcohol) (IDAM), (*R*)-*N*-methyl-(2-iodo-phenoxy)-3-phenylpropylamine (INXT), and (*N*-(3′-iodopropen-2′-yl)-2-beta-carbomethoxy-3-beta-(4-chlorophenyl)tropane) (IPT) were radiolabeled with ^{125}I by a method reported previously (*22,23*), with greater than 98% purity and a specific activity of 81 GBq/μmol.

Chemical Synthesis

General Procedure for Alkylation of Compound ***5*** *(5-Hydroxy-N,N-Dimethyl-2-(2-Nitrophenylthio)Benzamide).* The procedure for preparation of the derivatives of compounds **1** and **2** (Fig. 1) was reported previously (*20*). A solution of compound **5** (0.239 mmol) and bromo-fluoroalkane (**6/7**) or bromo-alcohol (**10/11**) (0.32 mmol) in *N,N*-dimethylformamide (10 mL) was added to potassium carbonate (3–4 molar equivalents). The mixture was heated at 110°C overnight, added to water (50 mL), and extracted with ethyl acetate (20 mL × 2). The organic layer was dried (Na_2SO_4) and purified by use of a silica gel column to yield a yellow oil. Alternatively, the reaction was accomplished with microwaves (Biotage Initiator) at 150°C for 15 min with a 83% yield, followed by the work-up described earlier to give the desired product. 5-(4-Fluorobutoxy)-*N,N*-dimethyl-2-(2-nitrophe-

nylthio)benzamide (**8**): ^{1}H NMR ($CDCl_3$) δ 8.18 (dd, J = 8.2, 1.5 Hz, 1H), 7.49 (d, J = 8.4 Hz, 1H), 7.40–7.32 (m, 1H), 7.23–7.14 (m, 1H), 7.01–6.92 (m, 3H), 4.54 (dt, J = 47.3, 5.4 Hz, 2H), 4.10 (t, J = 7.3 Hz, 2H), 3.02 (s, 3H), 2.86 (s, 3H), 1.99–1.78 (m, 4H). HRMS calculated for $C_{19}H_{22}FN_2O_4S$ [M^+ + H] 393.1284, observed 393.1256. 5-(5-Fluoropentyloxy)-*N,N*-dimethyl-2-(2-nitrophenylthio)benzamide (**9**): ^{1}H NMR ($CDCl_3$) δ 8.18 (dd, J = 8.2, 1.5 Hz, 1H), 7.48 (d, J = 8.5 Hz, 1H), 7.39–7.32 (m, 1H), 7.23–7.14 (m, 1H), 7.00–6.91 (m, 3H), 4.49 (dt, J = 47.2, 5.8 Hz, 2H), 4.03 (t, J = 6.2 Hz, 2H), 3.02 (s, 3H), 2.86 (s, 3H), 1.94–1.78 (m, 3H), 1.74–1.61 (m, 3H). HRMS calculated for $C_{20}H_{24}FN_2O_4S$ [M^+ + H] 407.1441, observed 407.1475. 5-(4-Hydroxybutoxy)-*N,N*-dimethyl-2-(2-nitrophenylthio)benzamide (**12**): ^{1}H NMR ($CDCl_3$) δ 8.18 (dd, J = 8.2, 1.5 Hz, 1H), 7.48 (d, J = 8.5 Hz, 1H), 7.40–7.35 (m, 1H), 7.22–7.14 (m, 1H), 7.01–6.92 (m, 3H), 4.07 (t, J = 6.1 Hz, 2H), 3.74 (t, J = 6.1 Hz, 2H), 3.02 (s, 3H), 2.86 (s, 3H), 2.00–1.86 (m, 2H), 1.83–1.66 (m, 2H). HRMS calculated for $C_{19}H_{23}N_2O_5S$ [M^+ + H] 391.1328, observed 391.1328. 5-(5-Hydroxypentyloxy)-*N,N*-dimethyl-2-(2-nitrophenylthio)benzamide (**13**): ^{1}H NMR ($CDCl_3$) δ 8.18 (dd, J = 8.2, 1.5 Hz, 1H), 7.48 (d, J = 8.5 Hz, 1H), 7.40–7.31 (m, 1H), 7.22–7.14 (m, 1H), 7.00–6.91 (m, 3H), 4.03 (t, J = 6.1 Hz, 2H), 3.68 (t, J = 6.1 Hz, 2H), 3.02 (s, 3H), 2.86 (s, 3H), 1.93–1.80 (m, 2H), 1.74–1.56 (m, 4H), 1.33 (t, 1H). HRMS calculated for $C_{20}H_{25}N_2O_5S$ [M^+ + H] 405.1484, observed 405.1471.

Procedure for Simultaneous Reduction of Nitro and Amide Groups. To a solution of **8/9** (0.1 mmol) in tetrahydrofuran (THF) at 0°C, 1.0 M BH_3-THF (10–15 molar equivalents) was added. The mixture was heated to reflux for 4.5–5 h. After cooling down, 0.5 mL of concentrated HCl was cautiously added, and the solvent was removed in vacuo. Water (5 mL) was added to the residue, and the mixture was heated to reflux for 30 min. To the mixture, 1N NaOH was added to adjust the pH to basic (pH 10–11) and extracted with ethyl acetate (5 mL × 2). The organic layer was dried (Na_2SO_4) and purified by use of a silica gel column (2% methanol in dichloromethane to 5% methanol in dichloromethane). 2-(2-((Dimethylamino)methyl)-4-(4-fluorobutoxy)phenylthio)benzenamine (**3**): ^{1}H NMR ($CDCl_3$) δ 7.38 (dd, J = 8.1, 1.6 Hz, 1H), 7.19–7.10 (m, 1H), 6.94 (d, J = 8.5 Hz, 1H), 6.87 (d, J = 2.7 Hz, 1H), 6.72–6.62 (m, 3H), 4.50 (dt, J = 47.3, 5.4 Hz, 2H), 4.57 (brs 2H), 3.95 (t, J = 5.7 Hz, 2H), 3.54 (s, 2H), 2.30 (s, 6H), 1.96–1.76 (m, 4H). HRMS calculated for $C_{19}H_{26}FN_2OS$ [M^+ + H] 349.1750, observed 349.1775. 2-(2-((Dimethylamino)methyl)-4-(5-fluoropentyloxy)phenylthio)benzenamine (**4**): ^{1}H NMR ($CDCl_3$) δ 7.38 (dd, J = 8.0, 1.5 Hz, 1H), 7.19–7.10 (m, 1H), 6.95 (m, 2H), 6.72–6.64 (m, 3H), 4.46 (dt, J = 47.2, 5.5 Hz, 2H), 4.47 (brs 2H), 3.93 (t, J = 6.1 Hz, 2H), 3.59 (s, 2H), 2.32 (s, 6H), 1.83–1.52 (m, 6H). HRMS calculated for $C_{20}H_{28}FN_2OS$ [M^+ + H] 363.1906, observed 363.1910.

Procedure for Selective Reduction of Amide Group. To a solution of amides **12/13** (0.18 mmol) in THF (10 mL) at 0°C, 1.0 M BH_3-THF (5 molar equivalents) was added. The mixture was heated to reflux for 1.5–2 h. To the mixture, 0.5 mL of concentrated HCl was cautiously added, and the solvent was removed in vacuo. Water (5 mL) was added to the residue, and the mixture was heated to reflux for 30 min. To the mixture, 1N NaOH was added to adjust the pH to basic (pH 10) and extracted with ethyl acetate (5 mL × 2). The organic layer was dried (Na_2SO_4) and purified by use of a silica gel column (2% methanol in dichloromethane to 5% methanol in dichloromethane) to provide the product as a yellow oil. 4-(3-((Dimethylamino)methyl)-4-(2-nitrophenylthio)phenoxy)butan-1-ol (**14**): ^{1}H NMR ($CDCl_3$) δ 8.24 (dd, J = 8.2, 1.5 Hz, 1H), 7.47 (d, J = 8.5 Hz, 1H), 7.34–7.26 (m, 2H), 7.22–7.13 (m, 1H), 6.87 (dd, J = 8.5, 2.9 Hz, 1H), 6.66 (dd, J = 8.0 Hz, 1.4 Hz, 1H), 4.01 (t, J = 6.1 Hz, 2H), 3.78 (t, J = 6.1 Hz, 2H), 3.48 (s, 2H), 2.18 (s, 6H), 2.00–1.69 (m, 4H). HRMS calculated for $C_{19}H_{25}N_2O_4S$ [M^+ + H] 377.1535, observed 377.1520. 5-(3-((Dimethylamino)methyl)-4-(2-nitrophenylthio)phenoxy)pentan-1-ol (**15**): ^{1}H NMR ($CDCl_3$) δ 8.24 (dd, J = 8.1, 1.5 Hz, 1H), 7.46 (d, J = 8.5 Hz, 1H), 7.37–7.20 (m, 3H), 6.87 (dd, J = 8.4, 2.8 Hz, 1H), 6.67 (dd, J = 8.0 Hz, 1.4 Hz, 1H), 4.05 (t, J = 6.2 Hz, 2H), 3.70 (t, J = 5.6 Hz, 2H), 3.48 (s, 2H), 2.18 (s, 6H), 1.98–1.79 (m, 2H), 1.74–1.57 (m, 4H). HRMS calculated for $C_{20}H_{27}N_2O_4S$ [M^+ + H] 391.1692, observed 391.1681.

Procedure for Mesylation. To a solution of **14/15** (0.11 mmol) in dichloromethane (5 mL) and triethylamine (45 mg/62 μL, 0.44 mmol), methanesulfonyl chloride (30 mg, 0.26 mmol) was added. The solution was stirred at room temperature for 2 h and washed with water (2 mL) and brine (2 mL). The organic layer was dried (Na_2SO_4), and the solvent was removed in vacuo. The product was purified by use of a silica gel column (dichloromethane:methanol, 18:2) to give a yellow oil. 4-(3-((Dimethylamino)methyl)-4-(2-nitrophenylthio)phenoxy)butyl methanesulfonate (**16**): ^{1}H NMR ($CDCl_3$) δ 8.24 (dd, J = 8.1, 1.6 Hz, 1H), 7.47 (d, J = 8.5 Hz, 1H), 7.34–7.26 (m, 2H), 7.22–7.13 (m, 1H), 6.87 (dd, J = 8.5, 2.9 Hz, 1H), 6.66 (dd, J = 8.0 Hz, 1.4 Hz, 1H), 4.34 (t, J = 6.0 Hz. 2H), 4.01 (t, J = 5.6 Hz, 2H), 3.49 (s, 2H), 3.03 (s, 3H), 2.19 (s, 6H), 2.04–1.96 (m, 4H). HRMS calculated for $C_{20}H_{27}N_2O_6S_2$ [M^+ + H] 455.1311, observed 455.1338. 5-(3-((Dimethylamino)-methyl)-4-(2-nitrophenylthio)phenoxy)pentyl methanesulfonate (**17**): ^{1}H NMR ($CDCl_3$) δ 8.24 (dd, J = 8.1, 1.5 Hz, 1H), 7.47 (d, J = 8.5 Hz, 1H), 7.34–7.13 (m, 3H), 6.86 (dd, J = 8.4, 2.7 Hz, 1H), 6.66 (dd, J = 8.0 Hz, 1.3 Hz, 1H), 4.28 (t, J = 6.1 Hz. 2H), 4.05 (t, J = 5.4 Hz, 2H), 3.49 (s, 2H), 3.01 (s, 3H), 2.19 (s, 6H), 1.99–1.80 (m, 4H), 1.70–1.56 (m, 2H). HRMS calculated for $C_{21}H_{29}N_2O_6S_2$ [M^+ + H] 469.1467, observed 469.1474.

Radiochemistry

The same method of ^{18}F fluorination can be applied to all 4 compounds and was reported previously (*20*). In brief, labeling was done by a nucleophilic ^{18}F-fluoride substitution reaction on the corresponding mesylate precursor followed by reduction with $SnCl_2$. The desired ^{18}F-labeled compound was then purified by semipreparative high-performance liquid chromatography (HPLC) (Phenomenex Gemini C18 semipreparative column [10 × 250 mm, 5 μm]; CH_3CN:ammonium formate buffer [10 mM], 55:45; flow rate, 3 mL/min; retention time, 6–15 min). At the end of synthesis, radiochemical purity and specific activity were calculated by analytic HPLC (Phenomenex Gemini C18 analytic column [4.6 × 250 mm, 5 μm], CH_3CN:ammonium formate buffer [10 mM], 8:2; flow rate, 1 mL/min; retention time, 4.0–6.5 min). Specific activity was estimated by comparing the UV peak intensity at 254 nm of the purified ^{18}F-labeled product with that of the reference nonradioactive compound at a known concentration. Radiochemical yield was calculated by dividing activity of the final purified product by the activity (decay corrected) in the starting QMA cartridge (Waters Corp.). The final product was dried under an N_2 stream.

Binding Affinity Determination

Preparation of cell membrane homogenates and binding affinity determination assay procedures were reported previously (*21*). In brief, membrane homogenates of LLC-PK_1 cells stably transfected

with SERT, NET, or DAT were mixed with buffer, radioligand (0.1 nM ^{125}I-IDAM, 0.07 nM ^{125}I-2-INXT, or 0.08 nM ^{125}I-IPT, respectively) and a range of 10 concentrations (10^{-10}–10^{-5} M) of the compound to be evaluated. Nonspecific binding was defined with 2.5 μM McN5652, 3.2 μM nisoxetine, or 1.9 μM GBR12909, respectively.

Biodistribution Studies

While rats were under isoflurane anesthesia, ~1.9 MBq of ^{18}F-radiolabeled ligand in a 200-μL solution of bovine serum albumin (1 mg/mL) were injected into each rat via the left femoral vein. The rats were then sacrificed at selected times (2–120 min). For the determination of organ and regional brain distributions, the organs and brain regions of interest were dissected, weighed, and assayed for radioactivity content. For calculation of the target-to-nontarget ratios for brain regions, the cerebellum, which contains low levels of SERT, was used as the nontarget region. For pharmacologic blocking studies, a SERT-, NET-, or DAT-selective inhibitor (IDAM at 2 mg/kg, nisoxetine at 10 mg/kg, or GBR12909 at 2 mg/kg, respectively) dissolved in a 200-μL solution of bovine serum albumin (1 mg/mL) was injected via the right femoral vein 5 min before radioligand injection. The regional brain distribution was determined 2 h after injection of the radioligand.

Autoradiography

A rat under isoflurane anesthesia was injected via the femoral vein with 179 MBq of ^{18}F-**3**. At 60 min after intravenous injection, the brain was removed, placed in embedding medium (Tissue Tek), and frozen on powdered dry ice. Consecutive 20-μm coronal sections were sliced on a cryostat microtome, thaw-mounted on microscope slides, and air dried at room temperature. Slides containing the brain sections were exposed to film (Kodak BioMax MR) overnight. In a second autoradiographic experiment, an injection of nisoxetine (10 mg/kg) was given 5 min before the injection of ^{18}F-**3** (171 MBq) to examine whether ^{18}F-**3** has a NET-binding component.

PET

Approximately 37–59 MBq of the selected radioligand was injected through a catheter placed in the tail vein. Imaging was performed with a Philips Mosaic Animal PET imaging system. The image voxel size was 0.5 mm^3. Data acquisition commenced at the time of radioligand injection. Scans were acquired over a period of 4 h, taking 5 min per frame for the first 2 h and 15 min per frame for the last 2 h. Region-of-interest analysis was performed with AMIDE software (http://amide.sourceforge.net/) on reconstructed images. To examine the specificity of the radioligand for SERT, an injection of escitalopram (2 mg/kg), nisoxetine (10 mg/kg), or GBR12909 (2 mg/kg) was delivered through the previously placed catheter 75 min after radioligand injection.

RESULTS

Chemistry

Two new fluorinated diaryl sulfides were prepared which differ at the 4′-position by the length of the alkoxy chain. The synthesis of the 2 new ligands, 4′-fluorobutoxy (**3**) and 4′-fluoropentoxy (**4**) derivatives, are shown (Fig. 2A). The synthesis is achieved by using a similar scheme to obtain the intermediate key phenolic compound **5** (*20*). Alkylation of the free OH group of intermediate compound **5** with commercially available 4-bromo-1-fluorobutane (**6**) and 5-bromo-1-fluoropentane (**7**) produced the fluoroalkoxy compounds, **8** and **9**, in 82% and 80% yields, respectively. The simultaneous reduction of nitro and amide groups of **8** and **9** with an excess of BH_3-THF furnished the desired compounds, **3** and **4**, in 60% and 62% yields, respectively.

Similarly, the synthesis of *O*-mesylate derivatives and their conversion to radiolabeled compounds ^{18}F-**3** and ^{18}F-**4** are shown in Figure 2B. In a manner similar to that used in earlier studies (*20*), phenolic compound **5** was alkylated with commercially available 4-bromo-butanol (**10**) and 5-bromo-pentanol (**11**) to produce compounds **12** and **13**, respectively, in quantitative yields. Selective reduction of the amide groups of **12** and **13** under controlled conditions furnished compounds **14** and **15** in 76% and 82% yields, respectively. The introduction of a methanesulfonyl group by reaction with methanesulfonyl chloride then provided the desired radiolabeling precursors, **16** and **17**, in quantitative yields.

Radiochemistry

As expected, the mesylate precursors were readily displaced by ^{18}F-fluoride in the presence of Kryptofix 222 (Sigma-Aldrich)–K_2CO_3 in acetonitrile. Total radiosynthesis time, including HPLC purification, was 75–90 min. Radiochemical yield was 6%–35%, radiochemical purity was greater than 97%, and specific activity ranged from 15 to 170 GBq/μmol (end of synthesis).

In Vitro Binding Affinity

It was found that the new 4′-4-fluorobutoxy-substituted (**3**) and 4′-5-fluoropentoxy-substituted (**4**) derivatives possessed subnanomolar binding affinities for SERT (inhibition constants, 0.51 and 0.76 nM, respectively) that were comparable to the binding affinities reported previously for compounds **1** and **2** (inhibition constants, 0.25 and 0.38 nM, respectively) (Fig. 3) (*21*). Compounds **1**, **2**, and **3** showed significant selectivity (30-fold) over NET, whereas compound **4** showed 9-fold selectivity. All 4 compounds had selectivity (>500-fold) over DAT.

In Vivo Biodistribution

For examination of SERT binding in vivo, the organ and regional brain distributions of the ^{18}F-radiolabeled compounds were measured. Some bone uptake was seen for ^{18}F-**1** and ^{18}F-**4**, but it declined over time (Table 1). Bone uptake did not decline for ^{18}F-**2** and declined only slightly for ^{18}F-**3** at 240 min, indicating possible in vivo defluorination. All 4 radioligands were able to successfully penetrate the blood–brain barrier and undergo significant washout from the brain by 120 min (Table 1). The results showed high initial brain uptake at 2 min for ^{18}F-**1**, ^{18}F-**2**, and ^{18}F-**3** (0.99–1.25 percentage injected dose per gram) and lower uptake for ^{18}F-**4** (0.68 percentage injected dose per gram). Over time, greater retention of activity was seen in the hypothalamus, whereas activity was quickly cleared from the background region, as represented by the cerebellum. At 120 min, the highest target-to-nontarget ratio (hypothalamus-to-cerebellum ratio) was

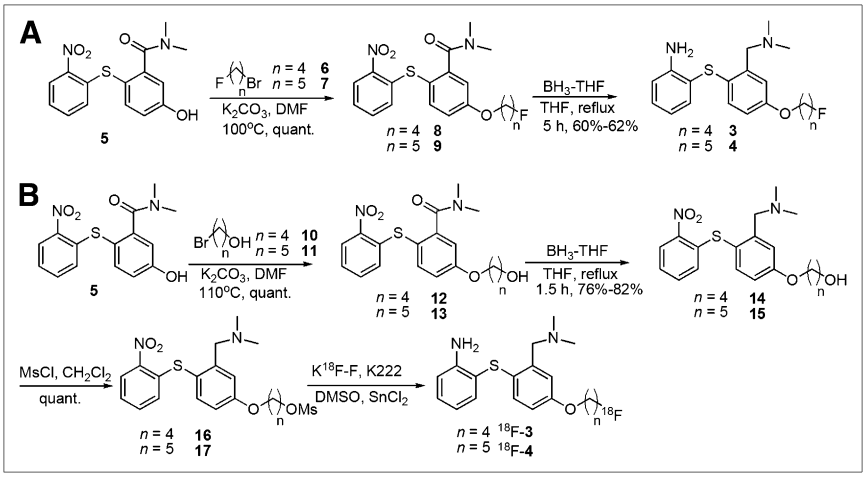

FIGURE 2. Preparation of nonradiolabeled (A) and radiolabeled (B) compounds. DMF = *N,N*-dimethylformamide; DMSO = dimethyl sulfoxide; K^{18}F-F = ^{18}F-fluoride; K222 = Kryptofix 222; MsCl = methanesulfonyl chloride; OMs = *O*-mesylate; quant. = quantitative yield.

seen for ^{18}F-**1**, at 7.83, with ^{18}F-**2** close, at 7.67. As chain length increased, the hypothalamus-to-cerebellum ratio decreased, with ^{18}F-**3** at 6.51 and ^{18}F-**4** at 5.70.

For confirmation that in vivo regional brain uptake was specifically attributable to SERT binding, pharmacologic blocking studies were performed. Pretreatment with the SERT-selective inhibitor, escitalopram, drastically reduced ^{18}F-**1**, ^{18}F-**2**, and ^{18}F-**3** binding to close to cerebellar levels in the striatum, hippocampus, cortex, and hypothalamus (Fig. 4). No effect or a minimal effect was seen in the cerebellum. Pretreatment with the NET-selective inhibitor, nisoxetine, caused a slight inhibition of ^{18}F-**1**, ^{18}F-**2**, and ^{18}F-**3** binding, but not in the cerebellum. Pretreatment with the DAT-selective inhibitor, GBR12909, was done with ^{18}F-**1** only. No inhibition was seen with GBR12909, and it is expected that similar results would be seen with ^{18}F-**2**, ^{18}F-**3**, and ^{18}F-**4**.

Ex Vivo Autoradiography

On the basis of the biodistribution results, ^{18}F-**1**, ^{18}F-**2**, and ^{18}F-**3** were selected for further evaluation by autoradiography. ^{18}F-**3** showed clear localization to SERT-rich regions, that is, the dorsal raphe, amygdala, thalamic nuclei, and hypothalamic nuclei (Fig. 5A). Pretreatment with nisoxetine did not appear to have an appreciable inhibitory effect; ^{18}F-**3** localization to the aforementioned regions was still present (Fig. 5B). Similar results were seen for ^{18}F-**1** (data not shown), and autoradiographic data for ^{18}F-**2** showing selective binding to SERT-binding sites in the rat brain were previously reported (*21*).

Small-Animal PET

PET was performed on rats after injection of ^{18}F-**1**, ^{18}F-**2**, or ^{18}F-**3**. Clear localization of ^{18}F-**3** in the midbrain, thalamus, and striatum was seen (Fig. 6). Nonspecific binding in the Harderian glands, commonly seen with other PET agents (*24*), was also present. There was minimal binding in the cerebellum, as expected (image not shown for ^{18}F-**1** and image reported previously for ^{18}F-**2** (*21*)).

Time–activity curves for ^{18}F-**3** were generated with AMIDE software (Fig. 7). The ratio of the brain region of interest to the cerebellum peaked at approximately 75–90 min and steadily declined afterward (Fig. 7A). Injection of escitalopram 75 min after tracer injection quickly reduced the ratio to starting levels (Fig. 7B). Nisoxetine injection appeared to cause some inhibition, but the decrease was not as marked as with escitalopram (Fig. 7C). Similar results were seen for ^{18}F-**1** and ^{18}F-**2** (data not shown). However, ^{18}F-**3** consistently displayed lower ratios of the brain region of interest to the cerebellum than ^{18}F-**1** or ^{18}F-**2**. An additional study with ^{18}F-**2** and

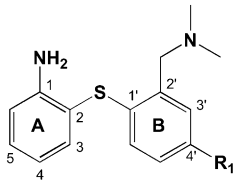

			K_i (nM)		
Compound	R_1	log*P*	SERT	NET	DAT
1	$O(CH_2)_2F$	2.15	0.25 ± 0.02	7.5 ± 0.7	340 ± 64
2	$O(CH_2)_3F$	2.54	0.38 ± 0.01	11.9 ± 1.7	299 ± 9
3	$O(CH_2)_4F$	2.87	0.51 ± 0.09	15.8 ± 1.3	486 ± 12
4	$O(CH_2)_5F$	3.14	0.76 ± 0.01	7.2 ± 0.7	397 ± 10

FIGURE 3. Log*P* and binding affinities of selected compounds for monoamine transporters. Compounds 1–4 all possessed strong binding affinity for their intended target, SERT, and excellent selectivity over DAT. These 4 compounds also showed some selectivity over NET.

TABLE 1. Biodistributions of ^{18}F-Labeled SERT Tracers in Male Sprague–Dawley Rats (n = 3) After Intravenous Injection

		^{18}F-**1**			^{18}F-**2***			^{18}F-**3**			^{18}F-**4**	
Parameter	Region	2 min	120 min	240 min	2 min	120 min	240 min	2 min	120 min	240 min	2 min	120 min
Distribution (% ID/g, mean ± SD)	Blood	0.54 ± 0.09	0.15 ± 0.04	0.08 ± 0.01	0.40 ± 0.04	0.14 ± 0.03	0.08 ± 0.01	0.41 ± 0.02	0.10 ± 0.02	0.05 ± 0.01	0.27 ± 0.04	0.07 ± 0.01
	Bone	0.20 ± 0.02	NA	0.07 ± 0.01	0.31 ± 0.06	0.26 ± 0.06	0.32 ± 0.02	0.35 ± 0.04	0.36 ± 0.03	0.25 ± 0.05	0.23 ± 0.04	0.15 ± 0.01
	Brain	1.02 ± 0.17	0.35 ± 0.08	0.07 ± 0.06	0.99 ± 0.08	0.39 ± 0.06	0.14 ± 0.02	1.25 ± 0.11	0.41 ± 0.06	0.08 ± 0.01	0.68 ± 0.09	0.24 ± 0.03
	HY	1.06 ± 0.23	0.74 ± 0.18	0.20 ± 0.06	1.15 ± 0.11	0.75 ± 0.18	0.34 ± 0.06	1.16 ± 0.04	0.70 ± 0.13	0.17 ± 0.03	0.61 ± 0.05	0.40 ± 0.05
	HP	0.99 ± 0.16	0.35 ± 0.10	0.06 ± 0.06	0.89 ± 0.06	0.38 ± 0.04	0.14 ± 0.02	1.05 ± 0.14	0.44 ± 0.05	0.09 ± 0.02	0.59 ± 0.10	0.25 ± 0.03
	CX	1.26 ± 0.19	0.43 ± 0.11	0.07 ± 0.03	1.05 ± 0.07	0.44 ± 0.08	0.12 ± 0.01	1.32 ± 0.25	0.53 ± 0.09	0.09 ± 0.01	0.78 ± 0.17	0.31 ± 0.04
	ST	1.01 ± 0.12	0.36 ± 0.05	0.08 ± 0.02	0.92 ± 0.04	0.46 ± 0.10	0.13 ± 0.00	1.15 ± 0.16	0.41 ± 0.05	0.07 ± 0.03	0.66 ± 0.12	0.26 ± 0.05
	CB	0.83 ± 0.10	0.09 ± 0.03	0.03 ± 0.00	1.02 ± 0.11	0.10 ± 0.02	0.03 ± 0.01	1.30 ± 0.07	0.11 ± 0.01	0.03 ± 0.00	0.65 ± 0.02	0.07 ± 0.01
Ratio of brain region to cerebellum (mean ± SD) calculated from % ID/g	HY/CB	1.28 ± 0.12	7.83 ± 0.49	6.58 ± 1.12	1.14 ± 0.15	7.67 ± 1.39	10.12 ± 3.44	0.90 ± 0.04	6.51 ± 0.49	6.42 ± 1.20	0.94 ± 0.05	5.70 ± 0.43
	HP/CB	1.19 ± 0.05	3.71 ± 0.26	2.14 ± 1.82	0.88 ± 0.07	3.87 ± 0.50	4.07 ± 0.88	0.81 ± 0.11	4.07 ± 0.20	3.30 ± 0.49	0.91 ± 0.13	3.63 ± 0.15
	CX/CB	1.53 ± 0.04	4.60 ± 0.46	2.44 ± 0.62	1.03 ± 0.12	4.53 ± 0.54	3.64 ± 0.91	1.02 ± 0.18	4.88 ± 0.34	3.26 ± 0.60	1.20 ± 0.23	4.41 ± 0.06
	ST/CB	1.22 ± 0.01	3.85 ± 0.66	2.72 ± 0.45	0.90 ± 0.12	4.67 ± 0.29	3.79 ± 0.64	0.89 ± 0.12	3.81 ± 0.35	2.75 ± 0.96	1.02 ± 0.16	3.68 ± 0.59

*Data for ^{18}F-**2** were reported previously (*22*) and are shown here for comparison.
NA = not available; HY = hypothalamus; HP = hippocampus; CX = cortex; ST = striatum; CB = cerebellum.

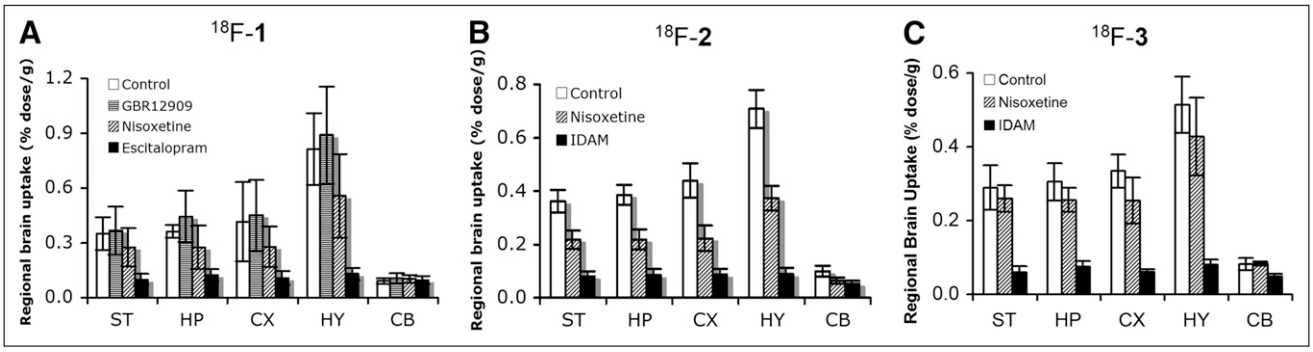

FIGURE 4. Effects of pretreatment with selective monoamine transporter inhibitors on regional brain distributions of ^{18}F-**1** (n = 3), ^{18}F-**2** (n = 6), and ^{18}F-**3** (n = 6). Rats were injected with sterile water, GBR12909 (DAT-selective inhibitor) at 2 mg/kg, nisoxetine (NET-selective inhibitor) at 10 mg/kg, escitalopram (SERT-selective inhibitor) at 2 mg/kg, or IDAM (SERT-selective inhibitor) at 2 mg/kg 5 min before ligand injection (1.1–1.8 MBq). Two hours after ligand injection, regional brain uptake was determined. Error bars indicate SDs. Escitalopram and IDAM considerably inhibited uptake into striatum (ST), hippocampus (HP), cortex (CX), and hypothalamus (HY). There was negligible inhibition with GBR12909, and there appeared to be some inhibition with nisoxetine. CB = cerebellum.

GBR12909 injection did not reveal any notable change compared with the results for the control (data not shown).

DISCUSSION

^{18}F ($t_{1/2}$, 109 min) provides a significant advantage over ^{11}C ($t_{1/2}$, 20 min). The longer $t_{1/2}$ of ^{18}F allows for off-site radioligand production and allows for more widespread clinical application. Currently, there still exists a need for SERT radioligands that possess the necessary properties for successful PET and that can be easily radiolabeled with ^{18}F. The first compounds synthesized, **1** and **2**, presented a novel placement of an alkoxy substituent on the 4′-position of ring B. This provided a site for simple ^{18}F radiolabeling that permitted relatively high radiochemical yields while maintaining high specific activity and a comparatively short synthesis time.

Along with ease of radiosynthesis, **1** and **2** proved to possess favorable radioligand properties for imaging SERT, such as good brain uptake and high target-to-nontarget ratios in vivo (*20,21*). With this discovery and the fact that ^{18}F-5-FADAM was reported to have a hypothalamus-to-cerebellum ratio of 12.49 at 2 h after injection in rat biodistribution studies, it was of interest to continue ligand development of this series and examine whether brain uptake and target-to-nontarget ratios could be further improved. Simple modification by increasing the length of the 4′-fluoroalkoxy chain was investigated. Increasing the chain length will predictably increase lipophilicity, but the effects on brain uptake and target-to-nontarget ratios are less clear. Thus, compounds **3** and **4** were synthesized, and the structure–activity relationships of the series were evaluated.

In vitro binding assays showed that the binding affinity profiles of **1**, **2**, **3**, and **4** essentially did not change with the alkoxy chain length. In vivo biodistribution studies showed that ^{18}F-**1** possessed the highest target-to-nontarget (hypothalamus-to-cerebellum) ratio (7.83), and increased chain length decreased this ratio. Whole-brain uptake was comparable for ^{18}F-**1**, ^{18}F-**2**, and ^{18}F-**3**; however, increasing the chain length to 5 carbons (^{18}F-**4**) decreased uptake. Accordingly, hypothalamic uptake of ^{18}F-**4** was also significantly

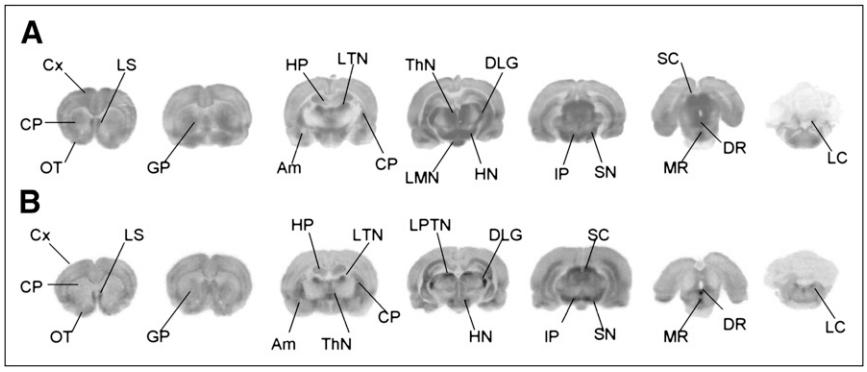

FIGURE 5. Ex vivo autoradiographs of ^{18}F-**3** in rat brain 60 min after ligand injection. (A) Control showed ^{18}F-**3** (179 MBq injected) localization to SERT-rich brain regions such as the amygdala (Am), thalamic nucleus (ThN), hypothalamic nucleus (HN), dorsal raphe (DR), and medial raphe (MR). (B) Nisoxetine (NET-selective inhibitor) pretreatment (10 mg/kg) had no appreciable effect on ^{18}F-**3** (171 MBq) binding. CP = caudate putamen; Cx = cortex; DLG = dorsal lateral geniculate nucleus; GP = globus pallidus; HP = hippocampus; IP = interpeduncular nucleus; LC = locus coeruleus; LMN = lateral mammillary nucleus; LPTN = lateral posterior thalamic nucleus; LS = lateral septum; LTN = lateral thalamic nucleus; OT = olfactory tubercle; SC = superior colliculus; SN = substantia nigra.

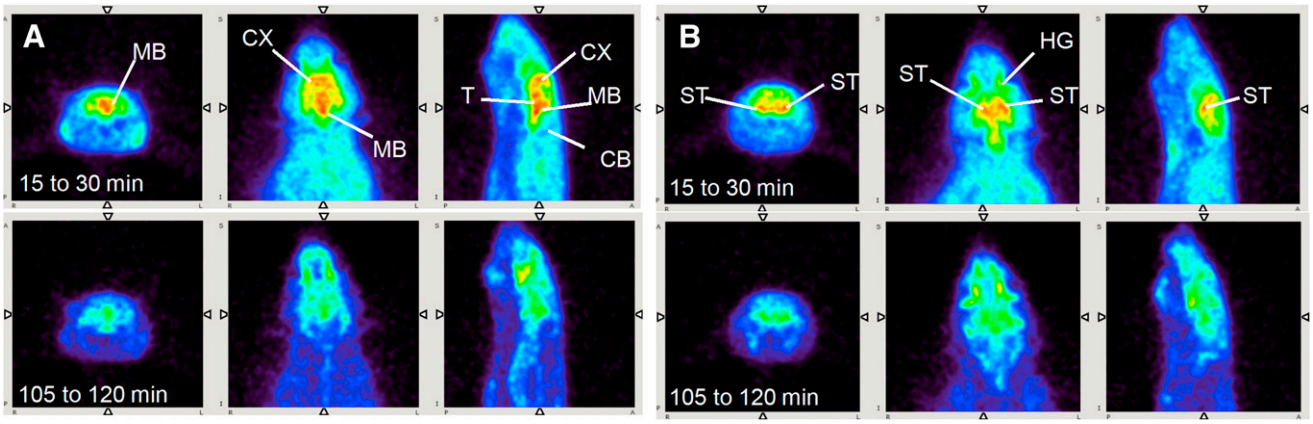

FIGURE 6. PET imaging in a normal control rat with ^{18}F-**3**. ^{18}F-**3** (52 MBq) was injected via tail vein into rat. Scanning immediately commenced after injection and was continued for 4 h. PET images (coronal, transverse, and sagittal views) show ^{18}F-**3** localization to areas known to contain SERT. (A) ^{18}F-**3** localization in midbrain (MB), cortex (CX), and thalamus (T). Little binding was seen in cerebellum (CB). (B) Different plane shows ^{18}F-**3** localization in striatum (ST). Nonspecific binding in Harderian glands (HG) is commonly observed in rats and mice for other PET agents (*24*).

decreased. Because of the lower brain uptake of ^{18}F-**4**, only ^{18}F-**1**, ^{18}F-**2**, and ^{18}F-**3** were selected for further studies.

In the pharmacologic blocking biodistribution studies, escitalopram clearly inhibited ^{18}F-**1**, ^{18}F-**2**, and ^{18}F-**3** binding in the striatum, hippocampus, cortex, and hypothalamus to levels similar to those seen in the cerebellum. The inhibition was expected because escitalopram is known to be a SERT-selective inhibitor. No further inhibition in the cerebellum was seen—an agreement with the fact that there is a very small amount of SERT in the cerebellum. Nisoxetine, a NET-selective inhibitor, also appeared to have some inhibitory effect, but like escitalopram, it had no inhibitory effect in the cerebellum. Escitalopram and nisoxetine are known to be highly selective for SERT (100,000-fold over NET) and NET (1,000-fold over SERT), respectively (*25,26*). If the inhibition seen with nisoxetine pretreatment was attributable to a NET-binding component, then incomplete inhibition by escitalopram in those 4 regions would be expected. This apparent inhibition by nisoxetine may have been attributable to indirect effects, such as an active metabolite or perhaps a consequential augmentation of serotonin levels, which could then displace the radioligand.

Furthermore, the time–activity curves generated from the PET images appeared to reveal some inhibitory effect of nisoxetine. A dual SERT and NET inhibitor chase experiment may be done to further examine whether additive inhibition would be seen beyond that of a SERT inhibitor alone. It should be noted that this phenomenon of nisoxetine inhibition was reported in a study by Ginovart et al. (*27*). They observed 78%−92% inhibition of ^{11}C-DASB binding after a nisoxetine dose of 2 mg/kg in cats in PET studies. They postulated that nisoxetine, a close structural analog of fluoxetine, may mediate inhibition by an active metabolite. When they tested a NET-selective inhibitor (500-fold over SERT) with a molecular structure dissimilar to that of fluoxetine, maprotiline, they did not see this inhibitory effect. They also stated that nisoxetine pretreatment did not affect ^{11}C-DASB binding in rats. A possible explanation for the difference in these studies may be the doses used. They used a dose of 2 mg/kg, whereas a dose of 10 mg/kg was used in the present study.

It is known that of the brain regions examined in these studies, the hypothalamus has the highest density of SERT and the cerebellum has the lowest. The hippocampus, striatum, and cortex have intermediate SERT densities (*28,29*). In the biodistribution studies, the highest ratio of the brain region of interest to the cerebellum was the hypothalamus-to-cerebellum ratio, suggesting that the lig-

FIGURE 7. Time–activity curves generated from PET image analysis with AMIDE software. Ratios of brain region to cerebellum are shown for ^{18}F-**3** (52–57 MBq). In selective inhibitor chase experiments, escitalopram or nisoxetine was injected 75 min after radiotracer injection (black arrows). (A) Control. (B) Escitalopram (2 mg/kg) rapidly and completely inhibited ligand binding. (C) Nisoxetine (10 mg/kg) appeared to have some inhibitory effect.

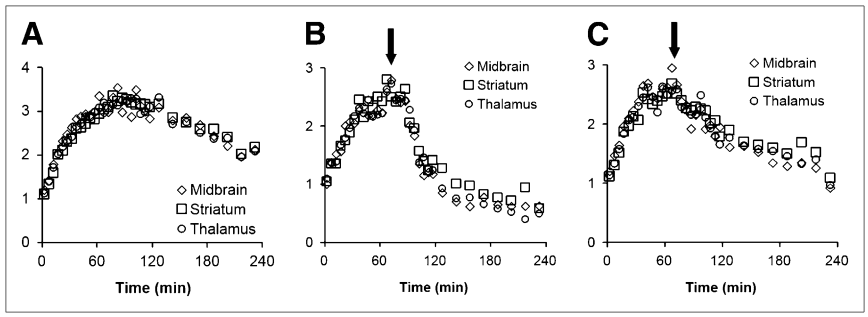

ands correctly targeted SERT in vivo. In addition, pretreatment with nisoxetine in autoradiographic studies did not seem to have a notable inhibitory effect on ligand binding, thus providing supporting evidence that the ligands selectively bound to SERT.

Thus, when ^{18}F-**1**, ^{18}F-**2**, ^{18}F-**3**, and ^{18}F-**4** were compared, it was found that ^{18}F-**4** had comparatively lower brain uptake and ratios of the brain regions of interest to the cerebellum in biodistribution studies and that ^{18}F-**3** had lower ratios of the brain regions of interest to the cerebellum in biodistribution and PET studies. Radiochemical yields for compounds **2**, **3**, and **4** were within similar ranges: 9%−25%, 6%−35%, and 6%−21%, respectively. Given the ease of synthesis, subnanomolar in vitro binding affinity, and positive small-animal PET results, ^{18}F-**1** and ^{18}F-**2** are the most promising agents in this series for PET studies of SERT. Additional PET studies of compounds **1** and **2** did not reveal one to be clearly superior to the other.

CONCLUSION

The 4 compounds presented all had a 4′-alkoxy chain that allowed for radiosynthesis to be performed under similar conditions with comparatively high radiochemical yields, specific activities, radiochemical purities, and short synthesis times. Furthermore, ^{18}F-**1**, ^{18}F-**2**, and ^{18}F-**3** displayed subnanomolar SERT affinities in vitro, in vivo selectivity, good brain uptake, and high target-to-nontarget ratios in rats. However, it was evident that ^{18}F-**1** and ^{18}F-**2** showed the most potential as successful ^{18}F-labeled PET agents for SERT, but because of cost restraints, only ^{18}F-**2** was chosen for further studies.

ACKNOWLEDGMENTS

This work was supported by National Institutes of Health grant R01-MH068782. PET imaging was performed at the Small-Animal Imaging Facility at the University of Pennsylvania. We thank Eric Blankemeyer for his technical expertise.

REFERENCES

1. Fergusson D, Doucette S, Glass KC, et al. Association between suicide attempts and selective serotonin reuptake inhibitors: systematic review of randomised controlled trials. *BMJ.* 2005;330:396.
2. Nemeroff CB. The burden of severe depression: a review of diagnostic challenges and treatment alternatives. *J Psychiatr Res.* 2007;41:189–206.
3. Meyer JH, Wilson AA, Sagrati S, et al. Serotonin transporter occupancy of five selective serotonin reuptake inhibitors at different doses: an [^{11}C]DASB positron emission tomography study. *Am J Psychiatry.* 2004;161:826–835.
4. Takano A, Suzuki K, Kosaka J, et al. A dose-finding study of duloxetine based on serotonin transporter occupancy. *Psychopharmacology (Berl).* 2006;185:395–399.
5. Meyer JH. Imaging the serotonin transporter during major depressive disorder and antidepressant treatment. *J Psychiatry Neurosci.* 2007;32:86–102.
6. Albin RL, Koeppe RA, Bohnen NI, Wernette K, Kilbourn MA, Frey KA. Spared caudal brainstem SERT binding in early Parkinson's disease. *J Cereb Blood Flow Metab.* 2008;28:441–444.
7. Bailer UF, Frank GK, Henry SE, et al. Serotonin transporter binding after recovery from eating disorders. *Psychopharmacology (Berl).* 2007;195:315–324.
8. Guttman M, Boileau I, Warsh J, et al. Brain serotonin transporter binding in non-depressed patients with Parkinson's disease. *Eur J Neurol.* 2007;14:523–528.
9. Rhodes RA, Murthy NV, Dresner MA, et al. Human 5-HT transporter availability predicts amygdala reactivity in vivo. *J Neurosci.* 2007;27:9233–9237.
10. Szabo Z, McCann UD, Wilson AA, et al. Comparison of (+)-^{11}C-McN5652 and ^{11}C-DASB as serotonin transporter radioligands under various experimental conditions. *J Nucl Med.* 2002;43:678–692.
11. Frankle WG, Huang Y, Hwang DR, et al. Comparative evaluation of serotonin transporter radioligands ^{11}C-DASB and ^{11}C-McN 5652 in healthy humans. *J Nucl Med.* 2004;45:682–694.
12. Jarkas N, Voll RJ, Williams L, Votaw JR, Owens M, Goodman MM. Synthesis and in vivo evaluation of halogenated *N,N*-dimethyl-2-(2′-amino-4′-hydroxymethylphenylthio)benzylamine derivatives as PET serotonin transporter ligands. *J Med Chem.* 2008;51:271–281.
13. Plisson C, Stehouwer JS, Voll RJ, et al. Synthesis and in vivo evaluation of fluorine-18 and iodine-123 labeled 2beta-carbo(2-fluoroethoxy)-3beta-(4′-((*Z*)-2-iodoethenyl)phenyl)nortropane as a candidate serotonin transporter imaging agent. *J Med Chem.* 2007;50:4553–4560.
14. Oya S, Choi SR, Coenen H, Kung HF. New PET imaging agent for the serotonin transporter: [^{18}F]ACF (2-[(2-amino-4-chloro-5-fluorophenyl)thio]-*N,N*-dimethylbenzenmethanamine). *J Med Chem.* 2002;45:4716–4723.
15. Garg S, Thopate SR, Minton RC, Black KW, Lynch AJ, Garg PK. 3-Amino-4-(2-((4-[^{18}F]fluorobenzyl)methylamino)methylphenylsulfanyl)benzonitrile, an F-18 fluorobenzyl analogue of DASB: synthesis, in vitro binding, and in vivo biodistribution studies. *Bioconjug Chem.* 2007;18:1612–1618.
16. Huang Y, Bae SA, Zhu Z, Guo N, Roth BL, Laruelle M. Fluorinated diaryl sulfides as serotonin transporter ligands: synthesis, structure-activity relationship study, and in vivo evaluation of fluorine-18-labeled compounds as PET imaging agents. *J Med Chem.* 2005;48:2559–2570.
17. Shiue GG, Choi SR, Fang P, et al. *N,N*-Dimethyl-2-(2-amino-4-^{18}F-fluorophenylthio)-benzylamine (4-^{18}F-ADAM): an improved PET radioligand for serotonin transporters. *J Nucl Med.* 2003;44:1890–1897.
18. Karramkam M, Dollé F, Valette H, et al. Synthesis of a fluorine-18-labelled derivative of 6-nitroquipazine, as a radioligand for the in vivo serotonin transporter imaging with PET. *Bioorg Med Chem.* 2002;10:2611–2623.
19. Plisson C, Jarkas N, McConathy J, et al. Evaluation of carbon-11-labeled 2beta-carbomethoxy-3beta-[4′-((*Z*)-2-iodoethenyl)phenyl]nortropane as a potential radioligand for imaging the serotonin transporter by PET. *J Med Chem.* 2006;49:942–946.
20. Parhi AK, Wang JL, Oya S, Choi SR, Kung MP, Kung HF. 2-(2′-((Dimethylamino)methyl)-4′-(fluoroalkoxy)-phenylthio)benzenamine derivatives as serotonin transporter imaging agents. *J Med Chem.* 2007;50:6673–6684.
21. Wang JL, Parhi AK, Oya S, Lieberman B, Kung MP, Kung HF. 2-(2′-((Dimethylamino)methyl)-4′-(3-[^{18}F]fluoropropoxy)-phenylthio)benzenamine for positron emission tomography imaging of serotonin transporters. *Nucl Med Biol.* 2008;35:447–458.
22. Goodman MM, Kung M-P, Kabalka GW, Kung HF, Switzer R. Synthesis and characterization of radioiodinated *N*-(3-iodopropen-1-yl)-2b-carbomethoxy-3b-(4-chlorophenyl)tropanes: potential dopamine reuptake site imaging agents. *J Med Chem.* 1994;37:1535–1542.
23. Kung MP, Hou C, Oya S, Mu M, Acton PD, Kung HF. Characterization of [^{123}I]IDAM as a novel single-photon emission tomography tracer for serotonin transporters. *Eur J Nucl Med.* 1999;26:844–853.
24. Kuge Y, Minematsu K, Hasegawa Y, et al. Positron emission tomography for quantitative determination of glucose metabolism in normal and ischemic brains in rats: an insoluble problem by the Harderian glands. *J Cereb Blood Flow Metab.* 1997;17:116–120.
25. Deupree JD, Montgomery MD, Bylund DB. Pharmacological properties of the active metabolites of the antidepressants desipramine and citalopram. *Eur J Pharmacol.* 2007;576:55–60.
26. Owens MJ, Morgan WN, Plott SJ, Nemeroff CB. Neurotransmitter receptor and transporter binding profile of antidepressants and their metabolites. *J Pharmacol Exp Ther.* 1997;283:1305–1322.
27. Ginovart N, Wilson AA, Meyer JH, Hussey D, Houle S. [^{11}C]-DASB, a tool for in vivo measurement of SSRI-induced occupancy of the serotonin transporter: PET characterization and evaluation in cats. *Synapse.* 2003;47:123–133.
28. Lin KJ, Yen TC, Wey SP, et al. Characterization of the binding sites for ^{123}I-ADAM and the relationship to the serotonin transporter in rat and mouse brains using quantitative autoradiography. *J Nucl Med.* 2004;45:673–681.
29. Xie T, Tong L, McLane MW, et al. Loss of serotonin transporter protein after MDMA and other ring-substituted amphetamines. *Neuropsychopharmacology.* 2006;31:2639–2651.